Supplementary Information (SI) for Journal of Materials Chemistry C.
This journal is © The Royal Society of Chemistry 2026

Impact of the core-substitution on the sequential reduction induced open-shell structures in Napthalenediimides

Amjed Khader K. T,[1] Arshad A,[1] Shant Chhetri,[1] Jesslyn John P, [1] Ratheesh K. Vijayaraghavan*[1]

[1] Department of Chemical Sciences, Indian Institute of Science Education and Research, Kolkata, Mohanpur 741246, Nadia, West Bengal, India.

Email: ratheesh@iiserkol.ac.in

1. Experimental section:

1.1. General methods:

UV-Vis absorption spectra in solution ($CHCl_3$) and film state were recorded using a 3 cm cuvette and quartz plate, respectively, using an Agilent Cary UV-Vis 3500 spectrometer. Spectro-electrochemistry, i.e., UV-Vis absorption spectral changes upon electrochemical reduction, were measured in a cuvette with 1mm optical path length. A sample solution (10μM) along with supporting electrolyte (1μM TBAPF6) was applied with continuous voltage using Pt mesh, Pt wire, and Ag/AgCl electrodes as the working, counter, and reference electrodes, respectively. Steady-state Photoluminescence (PL) spectra in solution were measured using an FLS-1000 Edinburgh Instrument with an Xe lamp source at 400 nm and a PMT detector, utilizing appropriate correction files. These samples were used for recording the decay profile. The fluorescence decay profile was performed using time-correlated single-photon counting (TCSPC) methods with HORIBA JOBIN S3 YVON (single photon counting controller: Fluorohub, precision photo multiplier power supply: Fluoro3PS). All simulation calculations were carried out using the Gaussian 16 program package and produced by UB3LYP/6-31G(d,p) method basis set. Field-emission scanning electron microscopy (FE-SEM) images were recorded using a ZEISS instrument (model no.: DSM 950). The samples were gold-coated, and the micrographs were taken using a scanning electron microscope (Zeiss DSM 950). The PXRD pattern was collected using a Rigaku Mini Flex diffractometer with Cu Kα radiation (λ = 1.540 Å). The tube voltage and amperage were set at 40 kV and 15 mA, respectively. The instrument was previously calibrated using a silicon standard. The vibrational modes present in the molecule were determined using solid-state ATR-FTIR spectra obtained from a Bruker Alpha Platinum ATR spectrophotometer.

1.2 Materials. All pristine reagents NDI-Br_o, NDI-Br_2 and NDI-Br_4 were prepared using a previously published procedure. The remaining solvents were procured from commercial suppliers (Sigma

Aldrich, Tokyo Chemical Industry) in the highest purity. Dry DCM (Ar/N_2-bubbled) was prepared to carry out Spectro-electrochemistry and EPR spectroscopy.

	Scanning potential	Characteristic peak
NDI-Br_0	-0.61V	478nm, 531nm, 751nm
NDI-Br_2	-0.48V	481nm, 524nm, 783nm
NDI-Br_4	-0.37V	489nm, 527nm, 785nm

Table S1: Spectro electrochemistry features upon applying the first reduction potential, a mono-radical is generated.

Generally, NDIs have an anionic peak around 470-490nm, while the dianion peak is broad, with a 450-600nm region.

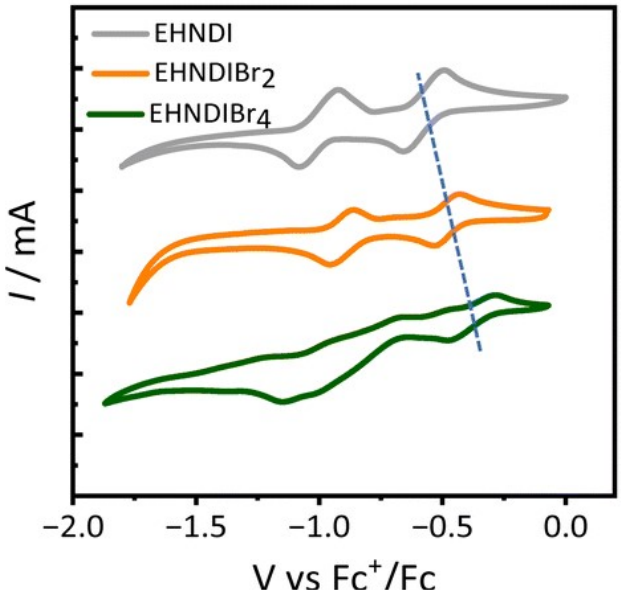

Figure S1. Cyclic voltammograms (reduction cycles) of NDI-Br_0, NDI-Br_2, and NDI-Br_4 recorded in CH_2Cl_2 (vs. Fc/Fc^+). Reproduced from Ref. [1][1] with permission from the Royal Society of Chemistry.

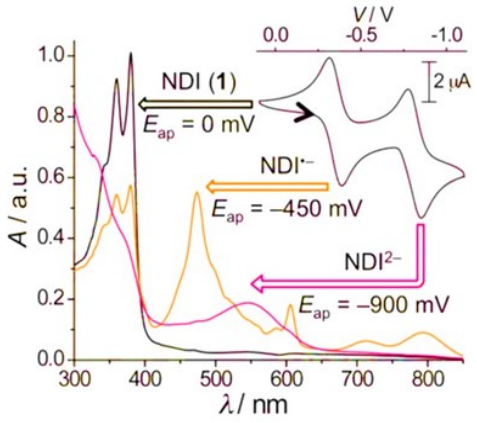

Figure S2: Cyclic voltammogram of a naphthalene diimide (NDI) derivative showing the first and second reduction waves, together with the corresponding UV–Vis spectro-electrochemical spectra assigned to the mono-radical and di-radical states. Adapted with permission from Ref. [2][2].

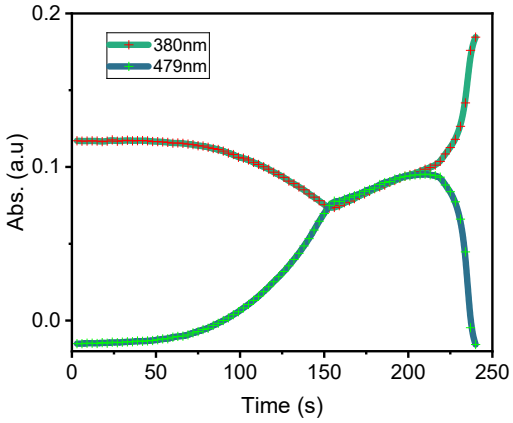

Figure S3: Time evolution of UV-Vis Abs. corresponding to ground state bleaching (380nm) and formation of mono-radical (479nm) of the NDI-Br_0 sample.

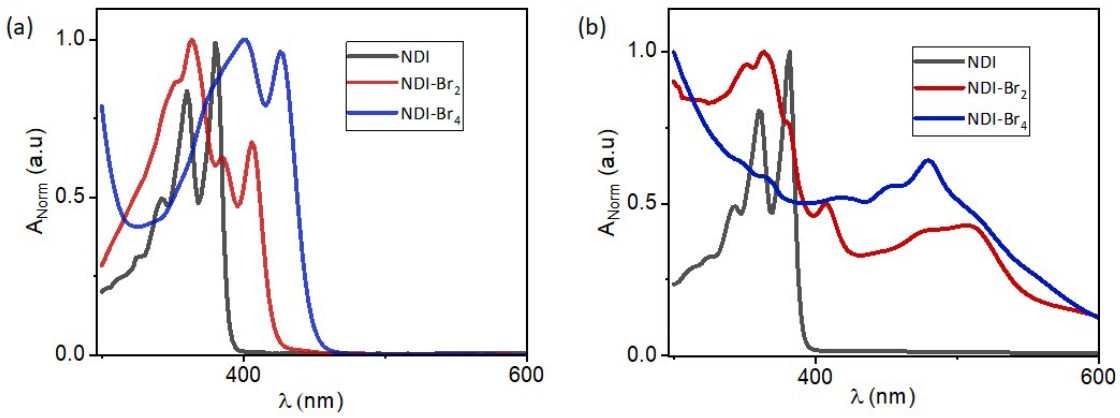

Figure S4: UV-Vis Absorption spectra of (a) pristine NDI (Br_0, Br_2, and Br_4) and (b) chemically Hz-treated samples. The concentration was approx. 2×10^{-5} mol L^{-1} in $CHCl_3$.

Here we have used the solvothermal synthesis approach at heating conditions (in the absence of an oxidant), which should facilitate anion/NDI-π interactions that trigger electron transfer from the anion to the NDI to generate $NDI^{\bullet-}$. The doped sample NDI-Br_4 revealed a sharp, intense absorption band centred at 478 nm, characteristic of a stabilized radical anion state. The sharper nature of this band underscores the strong localization and persistence of the radical, favored by extensive bromine substitution that substantially lowers the LUMO, thus enhancing both reducibility and radical yield.

Quantum Yield Calculation (relative method):

PLQY was determined using Rhodamine B in water (Φ_{ref}= 0.31) as a reference, with both reference and samples excited at 500 nm and measured under identical conditions. For each system, dilute solutions with A500 < 0.1 were prepared, integrated emission intensity was plotted versus absorbance, and the slope from a linear fit was obtained. The sample PLQY was then calculated as

The PLQY of the samples was calculated using:

$$\phi_{\text{sample}} = \phi_{\text{ref}}\left(\frac{S_{\text{sample}}}{S_{\text{ref}}}\right)\left(\frac{n_{\text{sample}}}{n_{\text{ref}}}\right)^2$$ where,

ϕ_{ref} is the known quantum yield of Rhodamine B in water, S_{sample} and S_{ref} are the slopes of integrated emission intensity versus absorbance for the sample and reference, and n_{sample} and n_{ref} are the refractive indices of DCM (1.424) and water (1.333), respectively.

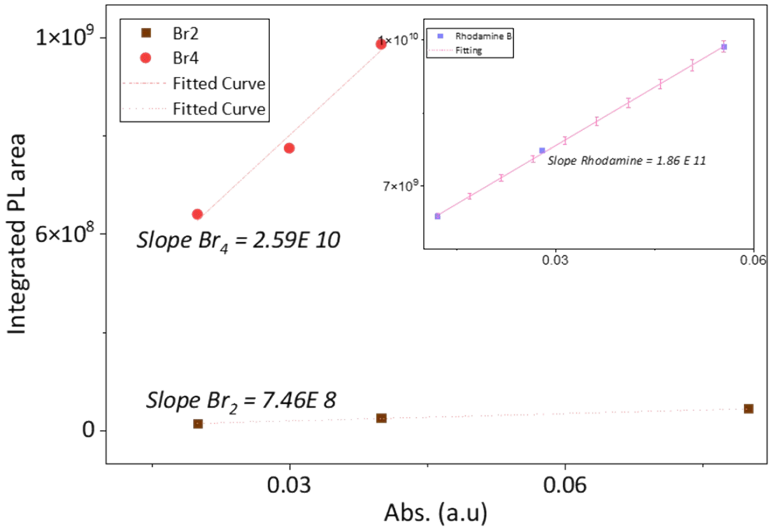

Figure S5. Linear dependence of integrated photoluminescence intensity on absorbance at the excitation wavelength for (a) Rhodamine B in water (inset) and (b) NDI-Br_2 and NDI-Br_4 in DCM. The slopes of the linear fits were used to determine relative quantum yields.

Where, slopes:

- $S_{\text{ref}} = 1.86 \times 10^{11}$ (Rhodamine B in water, $\Phi_{\text{ref}} = 0.31$)
- $S_{Br_2} = 7.46 \times 10^{8}$ (in DCM)
- $S_{Br_4} = 2.59 \times 10^{10}$ (in DCM)

Slope ratio:

Br_2: $S_{Br_2}/S_{\text{ref}} = 7.46 \times 10^{8}/1.86 \times 10^{11} \approx 0.00401$

Br_4: $S_{Br_4}/S_{\text{ref}} = 2.59 \times 10^{10}/1.86 \times 10^{11} \approx 0.139$

Refractive-index factor:
$(n_{\text{DCM}}/n_{\text{water}})^2 \approx (1.42/1.33)^2 \approx 1.14$

PLQY Calculations:

Using the relative slope method, incorporating the refractive index (n) of the solvents:

$\phi_{Br_2} = 0.31 \times 0.00401 \times 1.14 \approx 0.0014 = 0.14\%$

$\phi_{Br_4} = 0.31 \times 0.139 \times 1.14 \approx 0.049 = 4.9\%$

Sample	PLQY (%)
NDI-Br_2	0.14%

NDI-Br_4	4.9%

Wavelength-resolved lifetimes of Hz-doped NDI-Br_2

Time-resolved PL decays of Hz-doped NDI-Br_2 in solution were recorded at 540, 653, and 720 nm, and the corresponding average lifetimes are summarized.

Detection wavelength (nm)	Average lifetime ⟨τ⟩ (ns)
540	9.3
653	4.4
720	4.0

Table S2. Average fluorescence lifetimes of Hz-doped NDI-Br_2 at selected detection wavelengths.

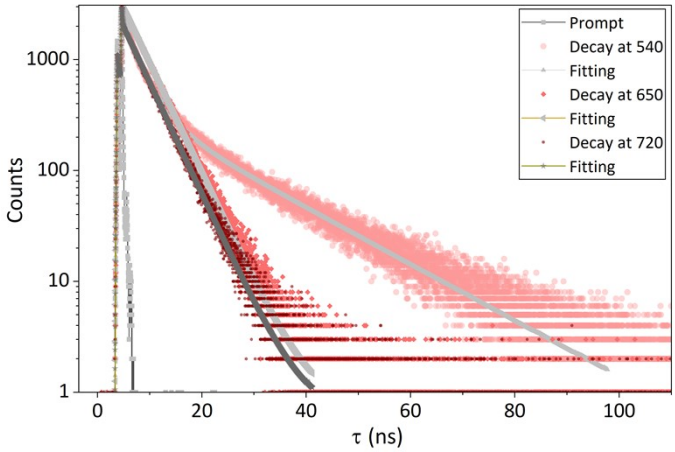

Figure S6. Normalised TCSPC decay curves of Hz-doped NDI-Br_2 in solution recorded at 540 nm, 653 nm, and 720 nm, with corresponding fits used to extract the average lifetimes listed in Table S2.

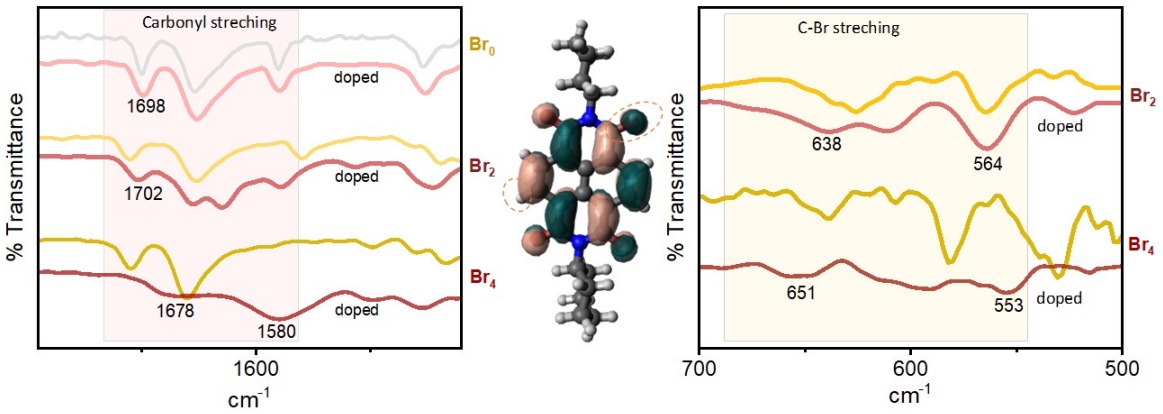

Figure S7: IR spectra (top), carbonyl stretching frequency of pristine and doped samples of NDI-Br_0 (top), NDI-Br_2 (centre), NDI-Br_4 (bottom), C-Br stretching frequency of pristine and doped samples of NDI-Br_2 and NDI-Br_4.

In NDI-Br_4, much more dramatic shifts were observed when compared to NDI-Br_2 and NDI-Br_0; the symmetric stretching band moved from 1661 to ~1609 cm^{-1} ($\Delta \approx 52$ cm^{-1}), and the asymmetric stretch shifted from 1712 to ~1688 cm^{-1} ($\Delta \approx 24$ cm^{-1}). These shifts reflect an increase in electron density around the carbonyl groups due to the formation of radical anions, which reduces the double bond character and lowers the stretching frequency. The magnitude of this shift can be correlated with the extent of reduction and localisation of charge density in the core, serving as a strong vibrational signature of radical ion formation. Upon doping with Hz, a significant loss or broadening of C-Br (550-650 cm^{-1}) is observed, suggesting electronic reorganization around the C-Br bond due to radical anion formation and altered bonding environments.

Spin density calculations:

	Energy (Hartee)
Br_0-neutral	-1576.20473373
Br_0-monoradical	-1576.26741859
Br_0-diradical	-1576.12506517

	Energy (Hartee)
Br_2-neutral	-6718.33862599
Br_2-monoradical	-6718.41381412
Br_2-diradical	-6718.29670267

	Energy (Hartee)
Br_4-neutral	-11860.51930271
Br_4-monoradical	-11860.60097231
Br_4-diradical	-11860.49710899

Table S3: Calculated energies of NDI (Br_0, Br_2, and Br_4) at ground-state optimized geometries using B3LYP/6-31G(d,p) for closed shell structure- neutral and UB3LYP/6-31G(d,p) for open shell structures (monoradical and diradical).

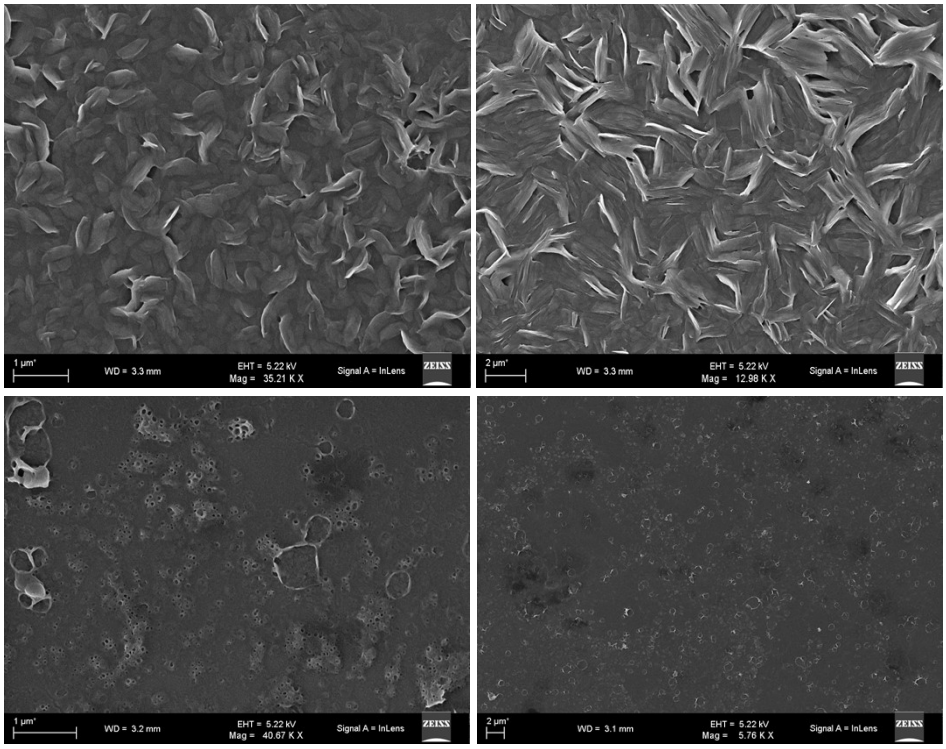

Figure S8: Pristine SEM image of Br_4 film (top) and hydrazine-doped Br_4 film (bottom).

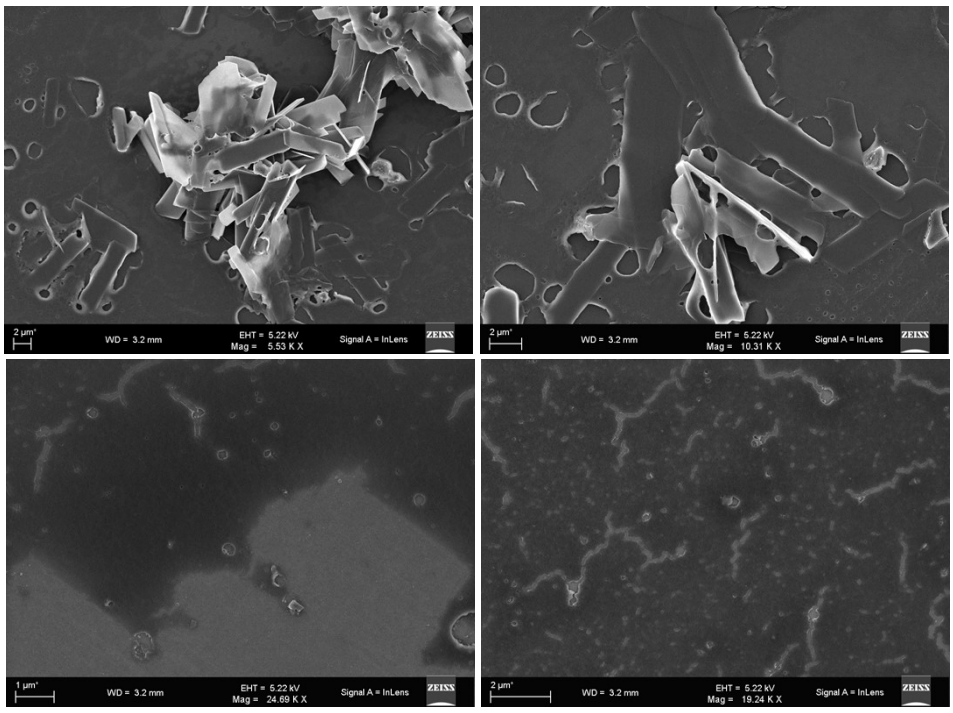

Figure S9: Pristine SEM image of Br_2 film (top) and hydrazine-doped Br_2 film (bottom).

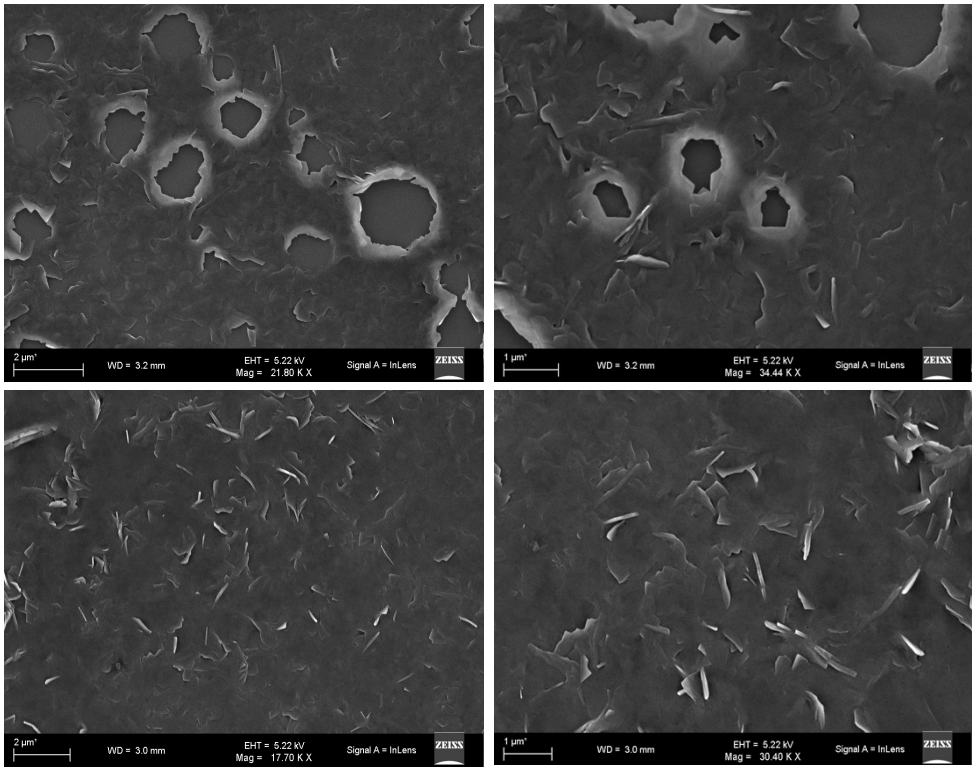

Figure S10: Pristine SEM image of Br_0 film (top) and hydrazine-doped Br_0 film (bottom).

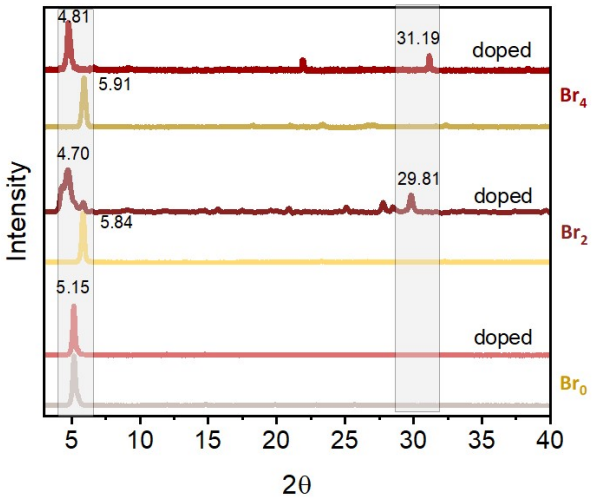

Figure S11: P-XRD pattern of pristine v/s doped NDI-Br_0 (down), NDI-Br_2 (middle), and NDI-Br_4 (up).

Compared to the neutral NDI, the NDI anion radical aggregates exhibited lower crystallinity and a shift in peaks to lower diffraction angles. This shift is likely to result from the insertion of the counterpart cation, leading to lattice expansion.

For Br_2 and Br_4, the photophysical measurements confirm the formation of persistent radical anion (and in Br_2 also dianion/delocalized) species, may be due to the presence of compensating cations and a modified solid-state packing of the reduced NDIs. A diffraction peak at $2\theta = 22°$ was also observed in Br_4 and is attributed to the π–π spacing between two adjacent backbones.

While the additional high-angle peaks can be attributed to a doped NDI radical ion phase with a distinct, more compact packing motif, accompanied with to structural rearrangements and new diffraction peaks observed for NDI radical anion salts and NDI-based radical crystals in the literature.[3] In contrast, NDI Br_0 does not form a stable reduced phase under the same conditions and therefore shows no new reflections.

REFERENCES

1 I. Giri, S. Chhetri, J. John P, M. Mondal, A. B. Dey and R. K. Vijayaraghavan, *Chem. Sci.*, 2024, **15**, 9630–9640.

2 S. Guha, F. S. Goodson, L. J. Corson and S. Saha, *J. Am. Chem. Soc.*, 2012, **134**, 13679–13691.

3 B. Kim, J. Lee, Y.-P. Chen, X.-Q. Wu, J. Kang, H. Jeong, S.-E. Bae, J.-R. Li, J. Sung and J. Park, *π-Stacks of radical-anionic naphthalenediimides in a metal-organic framework*, 2022.